Hindawi
International Journal of Antennas and Propagation
Volume 2019, Article ID 1934726, 7 pages
https://doi.org/10.1155/2019/1934726

Research Article

A Lumped-Element Decoupling and Matching Network for a Four-Element Mobile Handset MIMO Antenna

Riku Kormilainen, Rasmus Luomaniemi, Anu Lehtovuori, and Ville Viikari

Department of Electronics and Nanoengineering, Aalto University School of Electrical Engineering, P.O. Box 15500, Aalto 00076, Finland

Correspondence should be addressed to Ville Viikari; ville.viikari@aalto.fi

Received 25 June 2019; Accepted 4 October 2019; Published 23 October 2019

Academic Editor: N. Nasimuddin

This paper presents the first realization of a lumped-element decoupling and matching network (DMN) for more than two-element mobile MIMO arrays. The realization of the DMN is based on an existing method, which is improved in terms of bandwidth and the number of network elements. The array is designed to operate in the 2.6–2.7 GHz LTE band. The DMN is applied to a four-element MIMO antenna array located on one side of the mobile phone chassis. The array initially has a strong coupling of −3 dB, which is improved to −7 dB with the DMN. In other words, this denotes a reduction of 30 percentage points in coupled power. The DMN also improves the total efficiency by 21 percentage points at best.

1. Introduction

Growing data rates in recent years have made the use of MIMO technology a necessity in mobile communication. This trend increases the number of antennas required for mobile phones, which, along with shrinking available space, has created an issue with strong coupling between the antennas. In MIMO arrays, this strong coupling typically results in high channel correlation [1], which consequently lowers the MIMO capacity [2]. Hence, the issue of coupling has invoked interest in recent years. A popular research topic in the literature has been the decoupling and matching of two-antenna MIMO arrays for which there are a wide range of solutions. For example, solutions based on decoupling and matching networks (DMN) [3, 4], transmission line coupled resonators [5], LTCC filters [6], neutralization lines [7], scattering elements [8], defected ground structures [9], and antenna placement, location, and polarization [10] have been proposed.

Compared to two antenna arrays, analytical and straightforward lumped element network-based solutions are not so often used to coupling problems for larger MIMO arrays in mobile phones. In recent solutions, the antenna and decoupling structures are optimized with the help of laborious and time-consuming electromagnetic simulations. One example of such a solution is the design of a single antenna element with inherently low mutual coupling to other elements [11]. Other examples include use of parasitic metal strips [12, 13], neutralization lines [14], and lumped elements [15] between antennas as decoupling structures. The parasitic structures aim to decrease coupling by controlling the EM fields, whereas neutralization lines or lumped elements provide an alternate current path between antennas to cancel coupling. Besides decoupling structures, MIMO arrays consisting of antennas with orthogonal polarizations [16] and operating at different modes [17] have been proposed.

Since designing antennas and decoupling structures can be time consuming, solutions based on analytical approaches would be appreciated to accelerate the antenna design process. DMN is one of these straightforward approaches since the required circuit components can directly be calculated from scattering parameters. However, techniques for deriving DMN networks for N-element arrays are largely impractical due to the large number of lumped elements, cross connections, and a very narrow bandwidth [18, 19]. On the contrary, five different methods based on

antenna scattering parameters have been derived, and they aim to reduce the number of elements required for antenna arrays [20]. In hindsight, these methods still produce DMNs with cross connections and a very narrow bandwidth. Furthermore, their feasibility is severely limited since they assume that the lumped elements are ideally connected together.

In this paper, we use method 3 from [20] as a starting point for deriving a DMN for a four-element antenna array consisting of simple elements. We modify the DMN to take into account the bandwidth and the practical feasibility through element reductions and an iterative procedure. The reductions allow the manufacturing of the DMN on a single-layer PCB, and the procedure achieves a wider bandwidth with realistic element models in the DMN that is implemented on a real PCB layout. The effectivity of our approach is demonstrated by realizing a four-element mobile MIMO antenna array with a decoupling and matching network in the 2.6–2.7 GHz LTE band. Initially, mutual coupling is −3 dB at worst, but the DMN improves it to below −7 dB. The DMN also improves the total efficiency by 21 percentage points at best. This realization is the first time that a DMN is applied to mobile MIMO arrays with more than two elements.

2. Application of the Method

Figure 1 describes an N-element antenna array with a DMN, which can be presented as a $2N$-port admittance matrix block ($\mathbf{Y_D}$) connected to feeding ports (ports $1-N$ of $\mathbf{Y_D}$) and antennas ($\mathbf{Y_A}$) (ports from $N+1$ to $2N$ of $\mathbf{Y_D}$).

In general, the applied method [20] is based on partitioning this $2N$-port DMN admittance matrix into four submatrices as

$$\mathbf{Y_D} = \begin{bmatrix} \mathbf{Y_{D,11}} & \mathbf{Y_{D,12}} \\ \mathbf{Y_{D,21}} & \mathbf{Y_{D,22}} \end{bmatrix}. \tag{1}$$

When the admittance matrix is known, the network can be constructed with Π-circuits between all the ports. As implied by Figure 1, with N input and N output ports, $\mathbf{Y_D}$ is a $2N \times 2N$ matrix, and if all the matrix items are nonzero, the number of required components is $2N^2 + N$.

The submatrices of the DMN network can be computed with a few matrix operations. For brevity, we show only the necessary design equations of the method; the details can be seen in the original paper [20]. In order to define the DMN network, matrices $\mathbf{P}$ and $\mathbf{Q}$ are calculated with the help of an antenna scattering matrix ($\mathbf{S_A}$):

$$\mathbf{P} = \left(\mathbf{I} - \mathbf{S_A}\mathbf{S_A}^{\mathrm{H}}\right)^{-1}, \tag{2}$$

$$\mathbf{Q} = \mathbf{S_A}^{\mathrm{H}}\left(\mathbf{I} - \mathbf{S_A}\mathbf{S_A}^{\mathrm{H}}\right)^{-1}, \tag{3}$$

where $\mathbf{S_A}$ is the scattering matrix of the antenna array and $()^{\mathrm{H}}$ is the Hermitian transpose. Then, the following singular value decomposition is computed:

$$\mathbf{W\Sigma W}^{\mathrm{T}} = 2\mathrm{Re}\{\mathbf{P}\} + 2\mathrm{Re}\{\mathbf{Q}\} - \mathbf{I}, \tag{4}$$

where $()^{\mathrm{T}}$ is the transpose. After these computations, the submatrices of the DMN are as follows:

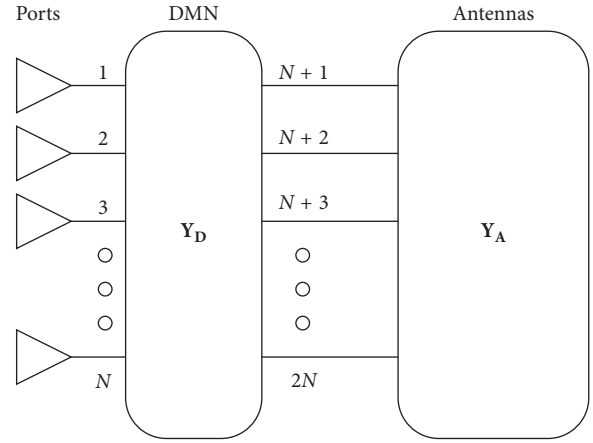

Figure 1: Block representation of an N-element antenna array with a DMN.

$$\mathbf{Y_{D,11}} = jY_0\mathbf{W}\left(\frac{1}{\sigma}\mathbf{\Sigma} - \mathbf{I}\right)^{1/2}\mathbf{W}^{\mathrm{T}}, \tag{5}$$

$$\mathbf{Y_{D,12}} = \mathbf{Y_{D,21}^{T}} = j\frac{Y_0}{\sqrt{\sigma}}\mathbf{I}, \tag{6}$$

$$\mathbf{Y_{D,22}} = jY_0\left[\frac{1}{\sqrt{\sigma}}\mathbf{W\Sigma}^{-(1/2)}\left(\mathbf{I} - \sigma\mathbf{\Sigma}^{-1}\right)^{1/2}\mathbf{W}^{\mathrm{T}} + 2\mathrm{Im}\{\mathbf{P} - \mathbf{Q}\}\mathbf{W\Sigma}^{-1}\mathbf{W}^{\mathrm{T}}\right], \tag{7}$$

where j is the imaginary unit, Y_0 is the port admittance, and σ is the smallest value on the diagonal of matrix $\mathbf{\Sigma}$.

Generally, the method diagonalizes $\mathbf{Y_{D,12}}$ and $\mathbf{Y_{D,21}}$, thus reducing the number of elements by $N^2 - N$ from the maximum. We apply the method to a four-element antenna array ($N = 4$) with a single symmetry plane. The method produces the following admittance matrix for the DMN:

$$\mathbf{Y_D} = \begin{bmatrix} Y_{11} & Y_{12} & Y_{13} & Y_{14} & Y_{51} & 0 & 0 & 0 \\ Y_{12} & Y_{22} & Y_{23} & Y_{13} & 0 & Y_{62} & 0 & 0 \\ Y_{13} & Y_{23} & Y_{22} & Y_{12} & 0 & 0 & Y_{62} & 0 \\ Y_{14} & Y_{13} & Y_{12} & Y_{11} & 0 & 0 & 0 & Y_{51} \\ Y_{51} & 0 & 0 & 0 & Y_{55} & Y_{56} & Y_{57} & Y_{58} \\ 0 & Y_{62} & 0 & 0 & Y_{56} & Y_{66} & Y_{67} & Y_{57} \\ 0 & 0 & Y_{62} & 0 & Y_{57} & Y_{67} & Y_{66} & Y_{56} \\ 0 & 0 & 0 & Y_{51} & Y_{58} & Y_{57} & Y_{56} & Y_{55} \end{bmatrix}. \tag{8}$$

Figure 2, illustrating the DMN component network, shows how these matrix values are applied to calculate the component values. Since our antenna array has a symmetry plane between antennas 6 and 7, the DMN network also exhibits symmetry along this plane. This symmetry is convenient in the optimization since the number of values to optimize decreases from 24 to 14.

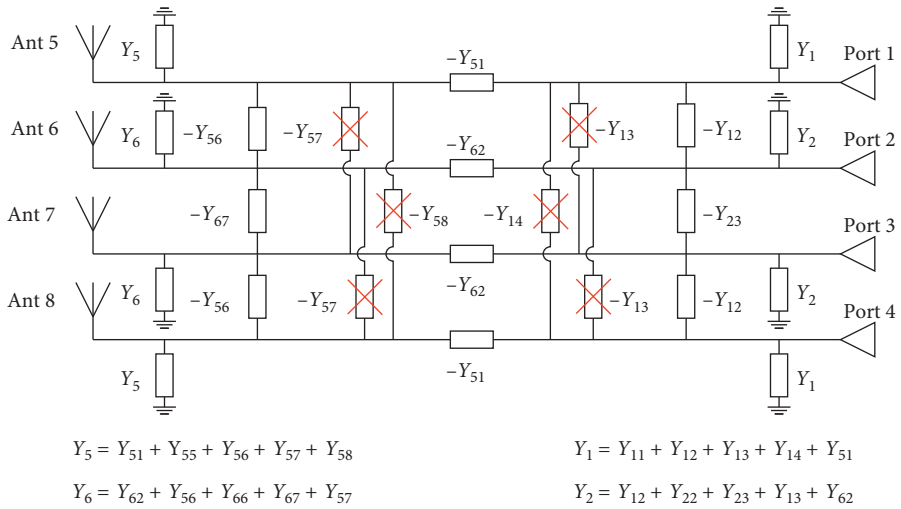

Figure 2: DMN network for a linear four-element antenna array.

3. Design of the MIMO Antenna Prototype

3.1. Initial Design of the Structure. In order to demonstrate the applicability of the method, we design a four-element MIMO antenna array in the 2.6 GHz–2.7 GHz LTE band. Figure 3 shows the prototype with dimensions, which are largely decided before the structural optimization. The size of the prototype is 73 mm by 148 mm, which is a typical size for a mobile phone. The substrate is low-loss Rogers RO4003C with a thickness of 1.524 mm. The ground plane is smaller with the dimensions of 69 mm by 140 mm. Thus, the clearances are 4 mm on the shorter sides and 2 mm on the longer sides. The four antennas are constrained to a single side and have a spacing of 1 mm. The antennas do not extend to the ends of the sides in order to leave space for 3G/4G/WLAN antennas on the shorter sides. The antennas are 0.1 mm thick and 4 mm high. The DMN components should be placed as close to each other as possible in order to minimize parasitic capacitances and inductances in the layout. Thus, feed ports are brought closer together with microstrip lines, which have a fixed minimum separation of 4 mm, a width of 1 mm, and a thickness of 35 μm.

In the initial structure optimization, the physical DMN, the ground patch, and the attachment patch (shown in Figures 3(a) and 3(c)) are omitted, and the feeding ports are implemented with discrete face ports between microstrips and the ground. Red dashed lines in Figure 3(c) show the feeding port locations. The structural optimization is performed by changing the lengths (l_{mid}, l_{out}) and feeding locations (d_{mid}, d_{out}) of the antennas. In the optimization, the goal is to minimize the reflection in the design band of 2.6–2.7 GHz. The antenna lengths after the optimization are 19 mm and 49.4 mm, and the feeding locations d_{mid} and d_{out} are 17 mm and 17.1 mm, respectively.

3.2. Optimizing the DMN without the Physical Network. As in the structural optimization, the antenna scattering parameters are simulated without the physical DMN, the ground patch, and the attachment patch. The obtained scattering parameters are applied in equations (2) and (3), which are then applied in equations (4)–(7) to calculate initial ideal component values. The cross connections, marked with red crosses in Figure 2, are removed to simplify the DMN design. This way, the DMN can be implemented on a single-layer PCB. Removing these components has a minor effect, as is verified by the results in Figure 4. The results with the full DMN (red solid line) and the reduced DMN (red dashed line) are very similar to each other across the 2.1–3.1 GHz band.

Next, the remaining elements are optimized to increase the minimum efficiency in the design band. Figure 4 also shows the matching efficiencies with the optimized values. The matching efficiencies (η_{match}) are calculated as

$$\eta_{\text{match}} = 1 - \sum_{n=1}^{N} |S_{nm}|^2, \tag{9}$$

where m is the number of the port and N is the number of the ports in the array. The optimization lowers the maximum matching efficiency but increases the minimum efficiency significantly. Compared to the case without the DMN, the lowest minimum efficiency increases from 40% to 63%, an increase of 23 percentage points.

3.3. Effects and Optimization of the Physical Network. When the physical DMN, the ground, the attachment patch, and a realistic feed are introduced, the operation of the DMN changes due to the parasitics introduced by the PCB layout. Figure 3(c) shows the implemented DMN, which has a total area of 10 mm by 9 mm. In the figure, the components are denoted as gray rectangles, and the red arrows show the new feeding locations. The actual realization is shown in Figure 5, which shows that the feed is implemented with semirigid coaxial cables that are grounded via the ground patch and are soldered to the attachment patch for additional measurement stability.

Because of the change in the DMN operation, a reoptimization is required. After the reoptimization, the

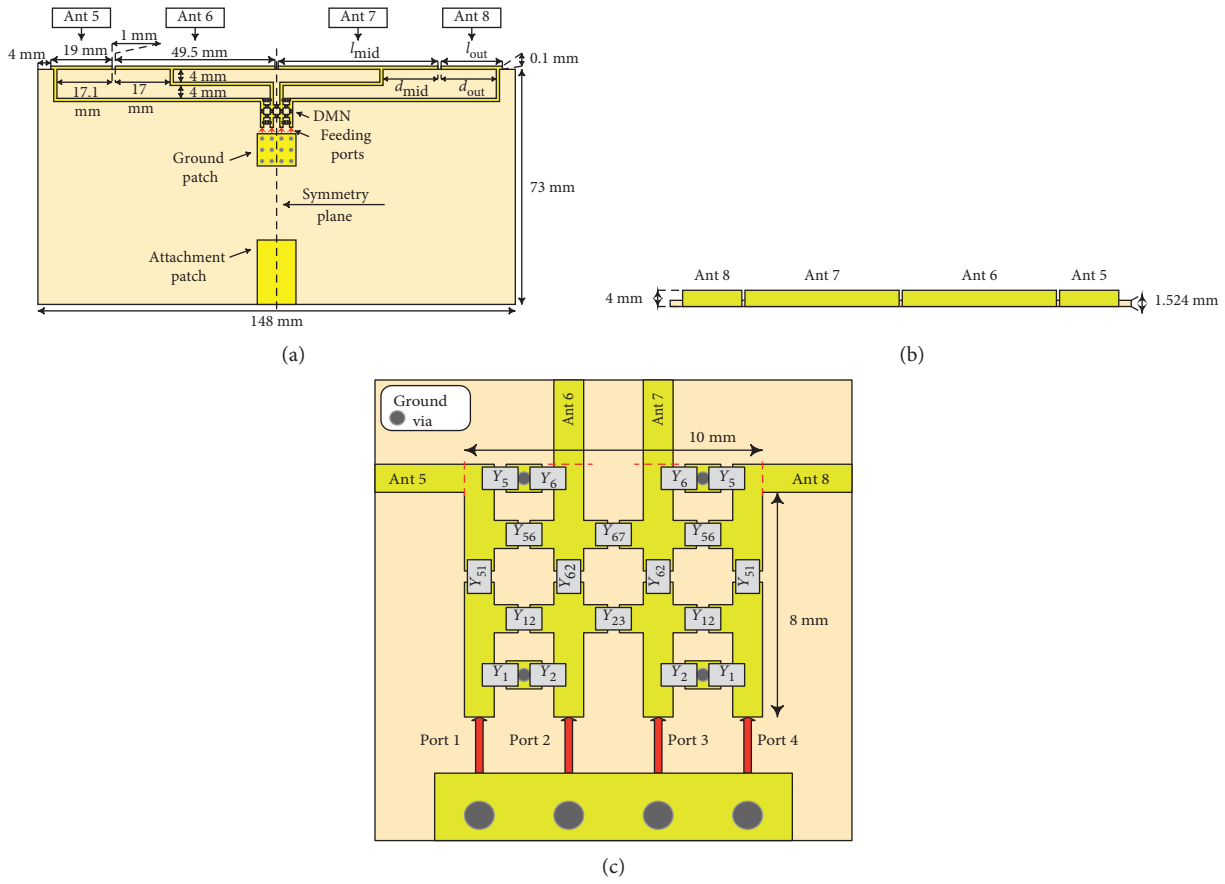

FIGURE 3: View of the prototype from the top (a) and front (b), and a close-up of the DMN (c). The gray rectangles denote lumped elements, the red arrows signify feeding locations, and the red dotted lines in the close-up are the feeding locations from the ground when the physical network is not included.

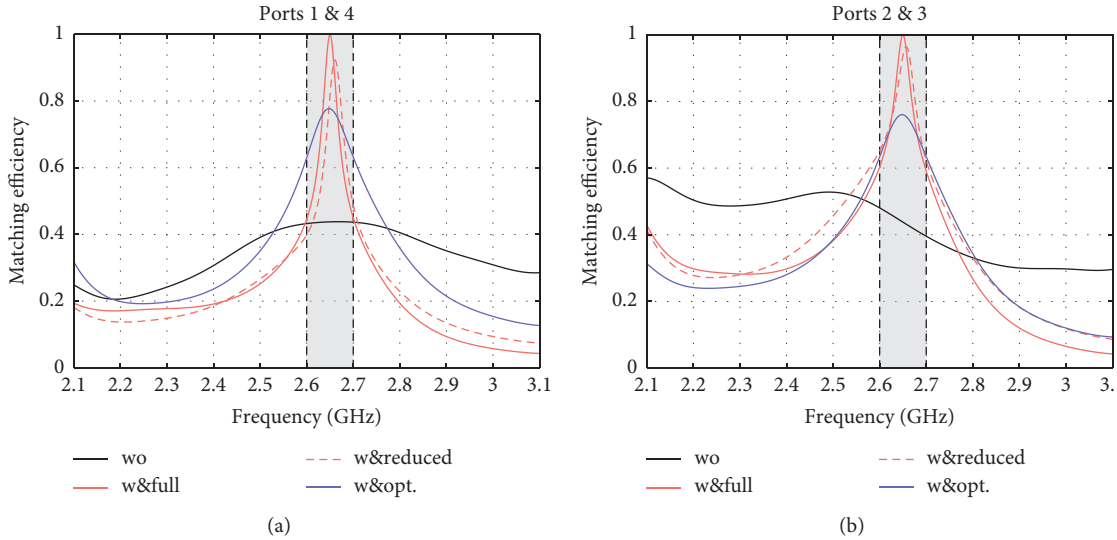

FIGURE 4: Matching efficiencies of the ports without the physical DMN. The results without (wo) the DMN and with the initially calculated full (w&full), reduced (w&reduced), and optimized (w&opt.) ideal DMN are shown.

matching efficiency is at least above 60% for all the ports in the design band. When ideal components are replaced with real Murata component models (series LQW15AN ∗ 80 and GJM1555C∗), yet another optimization is required. In this optimization, ideal elements are connected in parallel (for capacitors) or in series (for inductors) with the Murata

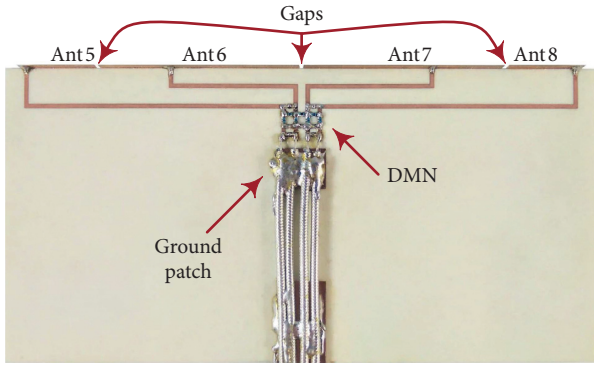

Figure 5: Top view of the manufactured prototype.

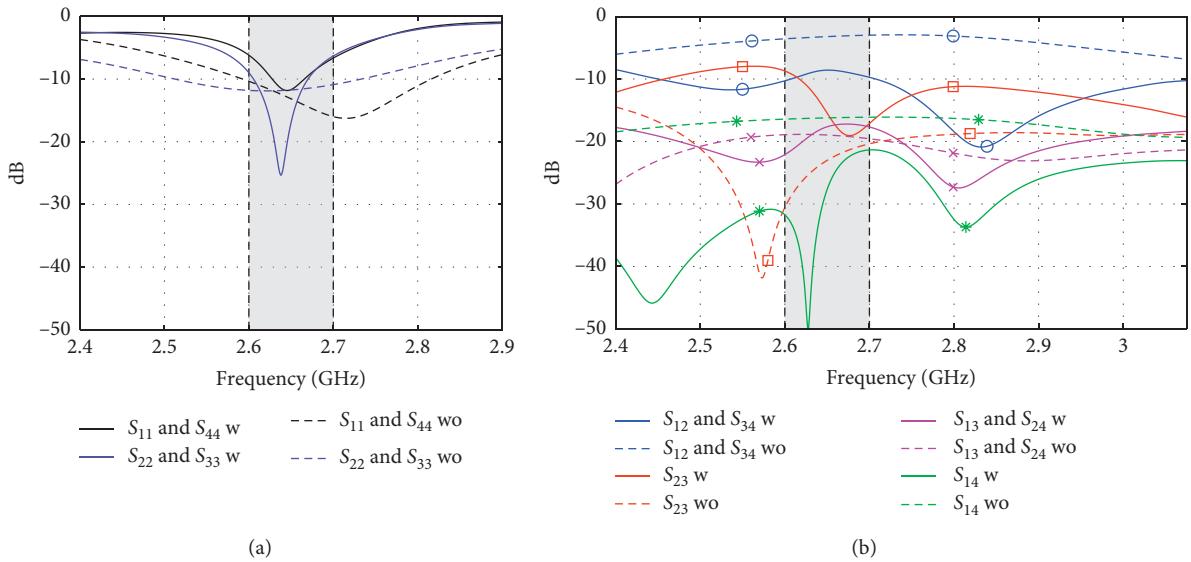

Figure 6: Simulated scattering parameters with (w) and without (wo) the DMN: (a) the reflection and (b) the coupling of the ports.

models. The ideal elements are optimized to define the values required in the real components. The optimization is performed simultaneously for all the elements. After this, the matching efficiency is at least 62%. Figure 6, showing the scattering parameters, reveals the reason for improved matching efficiency. The strongest couplings (S_{12} and S_{34}) improve from −3 dB to below −9 dB. This improvement comes at the price of increased coupling between middle antennas (S_{23}) and reflections (S_{ii}) at the ports. However, the improvements outweigh these deteriorations. This behavior is clearly visible, e.g., at 2.6 GHz. The reduced coupling between middle and outer antennas (S_{12} and S_{34}) decreases the power losses by 36 percentage points for all the ports. When the increased coupling of the middle antennas and reflections are taken into account, the DMN still reduce losses by 23 (ports 1 and 4) and 16 (ports 2 and 3) percentage points.

4. Measurements

The results of the simulated and measured matching and total efficiencies are shown in Figure 7. The total efficiency was measured with the MVG StarLab 6 GHz system in Aalto University. Figures 7(a) and 7(b) show that the measured matching efficiencies agree reasonably well with the simulated ones. The matching efficiencies of ports 1 and 4 (outer antennas) shift to higher frequencies, and the efficiencies of ports 2 and 3 (middle antennas) shift to lower frequencies. These small shifts are due to shifted resonance frequencies. Furthermore, the efficiencies of the middle and outer antennas are not identical, which are due to the differences in the measured S_{12} and S_{34}. These variations are explained by manufacturing tolerances, such as the amount of solder used, the component tolerances, and the variation in the spacing of the antennas. The prototype is rather sensitive to the DMN component values and spacing of antennas. Variations in either of these might cause relatively large changes in the S-parameters of the system.

The shifts and differences are also visible in the measured total efficiencies, which are shown in Figures 7(c) and 7(d) along with the simulated efficiencies with and without the DMN. The simulations suggest that the efficiencies increase between 12 and 20 percentage points for the outer antennas, whereas for the middle antennas, the increase varies between 6 and 23 percentage points. For the measured results, the maximum increases lie between 11 and 21 percentage points

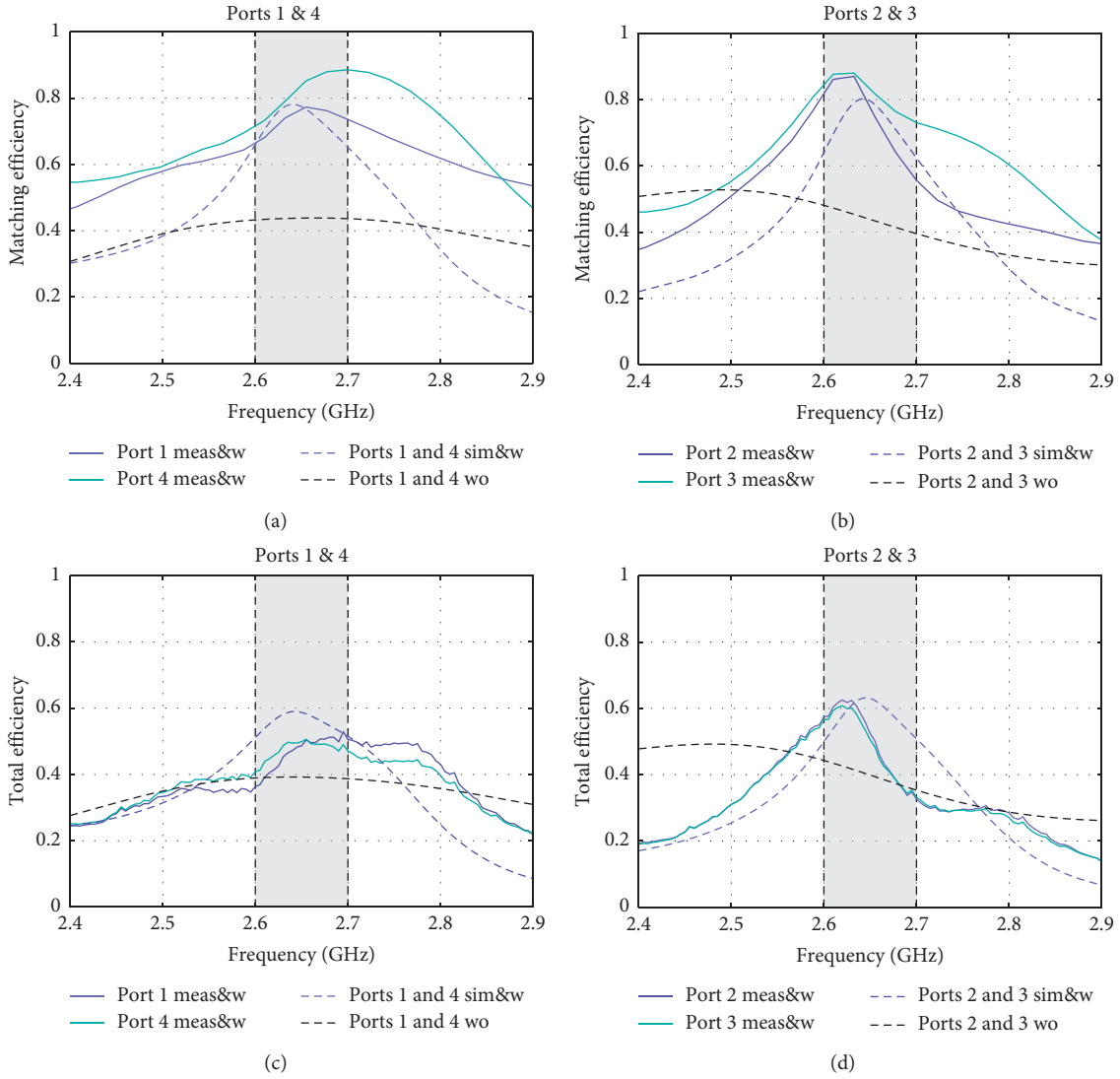

Figure 7: Measured and simulated matching and total efficiencies of the antennas. The simulated results with (sim&w) and without (wo) the DMN and the measured results with (meas&w) the DMN are shown.

Table 1: Comparison with other similar works.

Reference	Frequency (GHz)	Simulated total efficiency (%)	Antennas on a single side	Antennas in total
This work	2.6–2.7	>50	4	4
[12]	2.4–2.5	>40	2	4
[16]	2.55–2.65	>54	4	8
[13]	3.4–3.6	>60	2	4
[15]	3.4–3.6	>34	4	4
[11]	3.4–3.6	>62	4	8
[17]	3.4–3.6	>61	4	8
[14]	3.3–3.6	>46	4	8

for all the ports, which are relatively close to the simulation results. However, the lowest increase in the measured results is lower than expected. This is mainly due to the shifts.

Table 1 shows a comparison between this work and recent published articles that share similar mobile phone environment to our work. The table shows that this work fairs well compared with other works in terms of total efficiency. Although [11, 13, 17] report better efficiencies, they operate in a higher frequency band, where antenna sizes are smaller, and mutual coupling is therefore less of a problem.

5. Conclusion

In this paper, a lumped-element decoupling and matching network is realized for a four-element mobile MIMO antenna array based on an existing theoretical method. The DMN provided by the method is modified to take into account practical aspects. After the modifications, the DMN is operating in the 100 MHz band rather than at a point frequency. Furthermore, the modified DMN has fewer elements than originally, and it considers the physical layout promoting practical feasibility. The simulated and measured total efficiencies demonstrate that the modified DMN improves the performance of an array consisting of simple elements. The strongest coupling drops from −3 dB to −7 dB,

denoting a decrease of 30 percentage points in power losses. The results also show that DMNs are a practical choice for decoupling and matching antennas in mobile phones. They allow use of simple antennas, and their design is straightforward. Therefore, DMNs can alleviate the antenna design process reducing the need for complex decoupling structures, which can be laborious and time consuming to design.

Data Availability

The data used to support the findings of this study are included within the article.

Conflicts of Interest

The authors declare that they have no conflicts of interest.

Acknowledgments

This work was conducted within the 5G TRx project funded by Business Finland, Nokia Bell Labs, Huawei Technologies Finland, RF360, Pulse Electronics Finland, and Sasken Finland.

References

[1] P. Bahramzy, S. Svendsen, and G. F. Pedersen, "Isolation between three antennas at 700 MHz: for handheld terminals," *IET Microwaves, Antennas Propagation*, vol. 9, no. 3, pp. 237–242, 2015.

[2] M. A. Jensen and J. W. Wallace, "A review of antennas and propagation for MIMO wireless communications," *IEEE Transactions on Antennas and Propagation*, vol. 52, no. 11, pp. 2810–2824, 2004.

[3] X. Tang, K. Mouthaan, and J. C. Coetzee, "Tunable decoupling and matching network for diversity enhancement of closely spaced antennas," *IEEE Antennas and Wireless Propagation Letters*, vol. 11, pp. 268–271, 2012.

[4] C.-H. Wu, C.-L. Chiu, and T.-G. Ma, "Very compact fully lumped decoupling network for a coupled two-element array," *IEEE Antennas and Wireless Propagation Letters*, vol. 15, pp. 158–161, 2016.

[5] L. Zhao and K. L. Wu, "A dual-band coupled resonator decoupling network for two coupled antennas," *IEEE Transactions on Antennas and Propagation*, vol. 63, no. 7, pp. 2843–2850, 2015.

[6] H. Meng and K. L. Wu, "An LC decoupling network for two antennas working at low frequencies," *IEEE Transactions on Microwave Theory and Techniques*, vol. 65, no. 7, pp. 2321–2329, 2017.

[7] S.-W. Su and C.-T. Lee, "Printed two monopole-antenna system with a decoupling neutralization line for 2.4-GHz MIMO applications," *Microwave and Optical Technology Letters*, vol. 53, no. 9, pp. 2037–2043, 2011.

[8] B. K. Lau and J. B. Andersen, "Simple and efficient decoupling of compact arrays with parasitic scatterers," *IEEE Transactions on Antennas and Propagation*, vol. 60, no. 2, pp. 464–472, 2012.

[9] C.-Y. Chiu, C.-H. Cheng, R. D. Murch, and C. R. Rowell, "Reduction of mutual coupling between closely-packed antenna elements," *IEEE Transactions on Antennas and Propagation*, vol. 55, no. 6, pp. 1732–1738, 2007.

[10] H. Li, B. K. Lau, Z. Ying, and S. He, "Decoupling of multiple antennas in terminals with chassis excitation using polarization diversity, angle diversity and current control," *IEEE Transactions on Antennas and Propagation*, vol. 60, no. 12, pp. 5947–5957, 2012.

[11] A. Zhao and Z. Ren, "Size reduction of self-isolated MIMO antenna system for 5G mobile phone applications," *IEEE Antennas and Wireless Propagation Letters*, vol. 18, no. 1, pp. 152–156, 2019.

[12] H. Xu, H. Zhou, S. Gao, H. Wang, and Y. Cheng, "Multimode decoupling technique with independent tuning characteristic for mobile terminals," *IEEE Transactions on Antennas and Propagation*, vol. 65, no. 12, pp. 6739–6751, 2017.

[13] Z. Ren, A. Zhao, and S. Wu, "MIMO antenna with compact decoupled antenna pairs for 5G mobile terminals," *IEEE Antennas and Wireless Propagation Letters*, vol. 18, no. 7, pp. 1367–1371, 2019.

[14] W. Jiang, B. Liu, Y. Cui, and W. Hu, "High-isolation eight-element MIMO array for 5G smartphone applications," *IEEE Access*, vol. 7, pp. 34104–34112, 2019.

[15] C. Deng, D. Liu, and X. Lv, "Tightly-arranged four-element MIMO antennas for 5G mobile terminals," *IEEE Transactions on Antennas and Propagation*, vol. 67, no. 10, pp. 6353–6361, 2019.

[16] M.-Y. Li, Y.-L. Ban, Z.-Q. Xu et al., "Eight-port orthogonally dual-polarized antenna array for 5G smartphone applications," *IEEE Transactions on Antennas and Propagation*, vol. 64, no. 9, pp. 3820–3830, 2016.

[17] H. Xu, S. Gao, H. Zhou, H. Wang, and Y. Cheng, "A highly integrated MIMO antenna unit: differential/common mode design," *IEEE Transactions on Antennas and Propagation*, vol. 67, 2019.

[18] J. Weber, C. Volmer, K. Blau, R. Stephan, and M. A. Hein, "Miniaturized antenna arrays using decoupling networks with realistic elements," *IEEE Transactions on Microwave Theory and Techniques*, vol. 54, no. 6, pp. 2733–2740, 2006.

[19] J. Weber, C. Volmer, K. Blau, R. Stephan, and M. A. Hein, "Miniaturisation of antenna arrays for mobile communications," in *Proceedings of the European Microwave Conference*, pp. 1173–1176, Paris, France, October 2005.

[20] D. Nie, B. M. Hochwald, and E. Stauffer, "Systematic design of large-scale multiport decoupling networks," *IEEE Transactions on Circuits and Systems I: Regular Papers*, vol. 61, no. 7, pp. 2172–2181, 2014.